

Adhesion improvement and in vitro characterisation of 45S5 bioactive glass coatings obtained by atmospheric plasma spraying

B. Garrido, I.G. Cano, S. Dosta



PII: S0257-8972(20)31230-5

DOI: <https://doi.org/10.1016/j.surfcoat.2020.126560>

Reference: SCT 126560

To appear in: *Surface & Coatings Technology*

Received date: 27 August 2020

Revised date: 11 October 2020

Accepted date: 24 October 2020

Please cite this article as: B. Garrido, I.G. Cano and S. Dosta, Adhesion improvement and in vitro characterisation of 45S5 bioactive glass coatings obtained by atmospheric plasma spraying, *Surface & Coatings Technology* (2018), <https://doi.org/10.1016/j.surfcoat.2020.126560>

This is a PDF file of an article that has undergone enhancements after acceptance, such as the addition of a cover page and metadata, and formatting for readability, but it is not yet the definitive version of record. This version will undergo additional copyediting, typesetting and review before it is published in its final form, but we are providing this version to give early visibility of the article. Please note that, during the production process, errors may be discovered which could affect the content, and all legal disclaimers that apply to the journal pertain.

**Adhesion improvement and in vitro characterization of 45S5 bioactive glass coatings  
obtained by atmospheric plasma spraying**

B. Garrido, I. G. Cano, S. Dosta

<sup>a</sup>Thermal Spray Centre (CPT), Universitat de Barcelona (UB), 08028, Barcelona,  
Spain

**Sergi Dosta (\*Corresponding author)**

Email: [sdosta@ub.edu](mailto:sdosta@ub.edu)

c/Martí i Franqués 1. 08028 Barcelona, Spain

Telephone number: +34 93 402 12 97

**Abstract**

Plasma sprayed bioactive glass coatings were studied using crushed 45S5 bioactive glass powder. It is widely accepted that plasma sprayed coating microstructure is highly affected by the characteristics of the powder and the parameters set on the spraying process. Once the coating deposition was optimized, two strategies were carried out to analyse their effect on the coating adhesion: cooling with carbon dioxide while spraying and a post heat treatment to the as-sprayed coatings.

Scanning electron microscopy and X-ray diffraction were used for analyse the obtained coatings. Additionally, coating adhesion to the substrate and degradation of the coatings in Tris buffer solution were evaluated for the different samples studied.

Coatings have been tested in vitro to evaluate their response by immersion in simulated body fluid, Hank's Balanced Salt Solution.

The results show an increase in the adhesion strength for the heat treated samples due to the stress relaxation achieved above glass transition temperature. Moreover, in the bioactivity test an apatite layer at the coatings surface was produced for all the strategies studied.

*Keywords: bioactive glass, thermal spray, bioactivity, atmospheric plasma spray, coatings, biomaterials*

## 1. Introduction

The global market for orthopaedic devices which include joint reconstructions, spinal devices, orthobiologics (substitutes and bone grafts) and trauma fixation among others reach every year higher values. Several factors are increasing the demand for orthopaedic implants. Mainly the ageing of the population that cause bone related diseases as osteoporosis and osteoarthritis. But also other diseases connected to lack of physical activity or poor diet intake and obesity have a growing trend in the last years that increment the requests of implants. Moreover, the increasing incidence of road traffic accidents and sports injuries have been an important factor for the market. The global orthopaedic device market is expected to rise in the following years.

Orthopaedic devices are very successful but there is a rate of implant failure that ends in revision surgery to correct. It is important to consider that revision surgery takes much longer, and is less successful than the primary procedure. Also the cost is higher than the primary intervention. For the patient it means more pain and the recovery takes weeks or months. In addition to the risk of a new surgery [1].

The main failures for orthopaedic devices are related to infections, being trauma devices more affected than joint replacements [2]. Other complications are associated to the implant-tissue interface due to a non-sufficient osteointegration or the stress shielding caused by the mismatch between the mechanical properties of bone tissue and the implanted materials.

Current biomaterials are reaching their limits and there is a need for study new opportunities that can satisfy biomechanical and biological requirements to improve the long-term success and to reduce the risk for revisions of artificial implants. One option is functionalizing current materials with bioactive glass coatings.

In the late 1960s Larry Hench developed the first composition of bioactive glass, named 45S5. It was composed of the following oxides wt.%: sodium oxide (24.5%), calcium oxide



(24.5%), silicon dioxide (45.0%) and phosphorus pentoxide (6.0%). Takes its name because the glass has 45wt.% of  $\text{SiO}_2$  and a calcium to phosphorus molar ratio of 5:1 [3,4].

Bioactive glass materials are different from conventional glasses. Their structure is quite more disrupted than the conventional ones. Bioactive glasses are characterized by their bioactivity and their unique bone bonding properties related to their surface reactivity when immersed in aqueous medium [1,4,5]. Depending on the composition, the glass can bond also to the soft tissue. The mechanism for bone bonding is in consequence of the formation of hydroxycarbonate apatite (HCA) layer on the surface of the glass, resulting from the initial glass dissolution. The biological apatite is partially replaced by the bone after long-term implantation. It is due because the ion release products from bioactive glasses stimulate expressions of several genes of osteoblastic cells and promotes its proliferation [6–8]. Moreover, bioactive glasses show osteoconductive and osteoinductive capabilities [5].

The properties of each glass (e.g. the dissolution and the HCA layer formation rate) are a result of atomic structure. So by varying the content and the kind of the oxides in the glass, a full range of stability can be produced, from soluble to nonresorbable [1]. The 45S5 composition, in particular, is highly reactive.

When bioactive glasses come in contact with water, an ion exchange occurs at the glass/water interface. This ion exchange between modifier ions and protons from the solution results in a fast pH increase, mainly occurring in the first hours [9].

The release of ions from bioactive glasses is continuous over time [10], which suggest there is a release of ions from the bulk because the open silicate network allows the water molecules enter easy.

The excellent bioactive properties of bioactive glasses make them suitable for use to replace or repair damaged tissue. However, due to their poor mechanical properties, these glasses cannot be used as a bulk for load-bearing applications as other biomaterials such as titanium

and cobalt-chrome alloys. [6,11]. Otherwise, they are able to be used as bone grafts, scaffolds and coating materials.

The first clinical bioactive glass product, the “Bioglass® Ossicular Reconstruction Prosthesis”, was a device used to treat conductive hearing loss by replacing the bones of the middle ear. It was a structure intended to conduct sound from the tympanic membrane to the cochlea. For this product was used the 45S5 composition [3,12].

Nowadays, most of the bioactive glass products available in the market are bone grafts [13–15]. But there are some other applications like an absorbable composite interference screw of bioactive glass and PLLA-PDLLA or a component for toothpaste [16,17].

The current biomaterials used for load bearing applications meet the necessary mechanical requirements. However, they have an inert behaviour when implanted. For this reason is necessary to apply a superficial modification to improve their interaction with the body. There are several methods (physical, chemical or combined strategies) used to improve the bioactivity of the surfaces keeping at the same time the bulk properties unaltered. One of the strategies used to convert bioinert materials into bioactive ones is depositing a biomaterial that stimulates the implant and host bond integration by thermal spray techniques.

Plasma-sprayed HA coatings have been used as surface coatings on metallic implants since the 1980s [18]. Moreover, it is possible to find in the literature several studies of ceramics or glass coatings produced by different thermal spray techniques such as a coating of a HA and  $\text{TiO}_2$  mix (80-20% by weight) on  $\text{Ti}_6\text{Al}_4\text{V}$  by High-Speed Thermal Spray (HVOF) [19], biomimetic nanocrystalline apatites deposited by low pressure cold sprayed (LP-CS) on  $\text{Ti}_6\text{Al}_4\text{V}$  [20], apatite and wollastonite coatings by APS on  $\text{Ti}_6\text{Al}_4\text{V}$  [21], 45S5 bioactive glass by APS on AISI 304 metallic substrate [22], etc.

Several researchers have proposed bioactive glasses as an alternative to HA coatings because of their ability to create a stable interface that bond to bone strongly. Moreover, their dissolution products promote cells to differentiate to bone cells [7].

It is possible to find studies developing bioactive glasses coatings by different thermal spray processes [23–29]. Some of these studies use just the glass powder, others use suspensions, others solution precursors and there are also works where the glasses are mixed with other compositions. In most of the studies glass coatings are very defective and are weakly bonded to the substrate [30].

One of the major challenges of using bioactive glass as coatings is improving the adhesion of the coating [11]. In this article, different strategies were studied to develop plasma sprayed 45S5 bioactive glass coatings with better adhesion. First step was varying the spraying parameters to achieve the best adhesion directly from the technique. Then two different approaches were studied: a cooling process with carbon dioxide while spraying the powder and a heat treating of the samples after spraying. Achieving good adhesion of the coating to the substrate is essential for bioactive glasses to be considered candidates to replace current hydroxyapatite coatings.

## **2. Experimental methods**

### **2.1 Powder and substrate**

The 45S5 bioactive glass powder was obtained from Denfotex research (United Kingdom). The powder was produced by the traditional melt-quenching route. To the milled powder 0.7 wt.% of aerosil was added, as an extra in the standard formulation, mixing directly with the powder. This fumed silica (aerosil) serves as a universal anticaking agent in powders, to make powders capable of flowing during spray process.

Titanium grade V disks of 2mm thick and 9mm diameter (Tamec, Spain) were used as substrates for physical and biological characterization. Specimens with 25mm diameter were used to measure the adhesion strength of the coatings.

### **2.2 Coating deposition**

Bioactive glass coatings were deposited by Atmospheric Plasma Spraying (APS) onto titanium grade V substrates, previously grit blasted with corundum and then cleaned with ethanol before spraying.

The plasma spray equipment used was an APS A3000S system equipped with F4 Plasma torch. Argon was used as primary gas and hydrogen as secondary for the plasma plume formation. Powder carrier gas was also argon. The spraying parameters are listed in Table 1.

Spraying particles of brittle materials causes high stresses after solidification due to the rapid cooling. These stresses are relaxed through generating cracks, for this reason the coatings of glasses tend to present cracks and pores. Spraying parameters were studied to achieve a good melting of the particles to get homogeneous coatings. Stand-off distance was modified from 80 to 130mm, getting more controlled porosity for longer distances. Also the argon and hydrogen plasma gas flow rate has been changed from 30-35slpm and 12-6slpm, respectively. The carrier gas flow rate was adjusted from 4 to 6l/min, being the lower the more appropriate. The injection angles used in these trials were whether 90° or 75° backwards.

Trying to diminish the high stresses produced during solidification of the particles carbon dioxide was used in a cooling system fixed to the torch. Two nozzles on both sides of the spray torch emit a jet of carbon dioxide straight into the substrate during spraying. The idea is that particles arrive less heated to the substrate and diminish the amount of stresses that can affect the bond by the difference of temperature between the particles and the substrate. Carbon dioxide instead of air was chosen for cooling to ensure enough refrigeration and thus obtain glassy coatings. Afterwards we saw that cooling was not needed for obtain amorphous coatings.

In order to increase the bond adhesion a post heat treating was done to induce crystallinity and reduce the defects of the coating. The temperatures were selected in order to favour crystallization. At 610°C a process of crystallization takes place for the 45S5 composition, and another one around 800°C, these temperatures vary depending on the size particle or

thickness of the coating and the heating conditions [31]. Besides, the chosen temperatures were designated in a range where titanium alloy crystal structures remain unchanged [32]. The heating rate should be slow to avoid large temperature gradients and stresses which could result in cracking of the material. The as-sprayed coatings were heat treated at 725°C and 800°C for 5h and with a heating rate of 5°C/min in an air-circulated furnace, followed by slow cooling to room temperature.

### **2.3 Powder characterisation**

The powder was sieved to get a narrow range before spraying. Laser diffraction particle size analyser Beckman Coulter LS 13320 was used to study the granulometry of the powder.

The shape and surface morphology of the glass powder was determined using a scanning electron microscope (SEM), JEOL JSM-5310 equipment. The samples were coated by a gold layer before microscopy study.

### **2.4 Coating characterisation**

The crystal structure of the samples was determined by X-ray diffraction (XRD) using a PANalytical X'Pert PRO MPD Alpha1 powder diffractometer to define the structural changes caused by the processes.

The coatings and the formation of HCA layer on the surface of the samples after soaking in simulated body fluid were evaluated using SEM, JEOL JSM-5310 equipment.

The surface roughness of the final coatings was registered using a MITUTOYO SURFTEST 301. The Ra value corresponding to the arithmetical mean deviation of the assessed profile was recorded.

The adhesion strength of the coatings was measured according to ASTM C633-13 standard at atmospheric temperature. Coatings were glued using HTK ULTRA BOND 100® glue (HTK) to uncoated grit blasted samples. The tensile adhesion test was done using a Servosis ME-402/10 with self-aligning devices at 0.02mm/s of displacement rate and control of the position.

## 2.5 Bioactivity and degradation assessment

The in vitro ability to form apatite on the samples was studied following the ISO 23317:2014 using the simulated body fluid Hank's Balanced Salt Solution (HBSS) (Sigma-Aldrich, Germany). The composition of the HBSS is similar to the found in human blood plasma and some in vitro studies have been performed with this composition [33–35]. Coated samples were immersed in HBSS and exposed for 0, 1, 3, 6 and 14 days at 37°C in a thermostatic bath with agitation. The solution was changed every 3 days to avoid ionic saturation of the medium. After the soaking time, the samples were rinsed three times with ultrapure water and dried for 24h at room temperature.

Before and after immersion the samples were characterized using SEM coupled with EDS to analyse the chemical and physical changes related to the bone-like apatite formation.

A degradation study was performed by immersing the samples for 120h in a buffered solution consisting of Tris-HCl with pH adjusted to  $7.4 \pm 0.1$  at  $37 \pm 1^\circ\text{C}$  following the ISO 10993 standard, part 14: "Identification and quantification of degradation products of ceramic materials". The samples were placed in sterile polypropylene containers during the test. After degradation time, samples were rinsed thrice with ultrapure water and dried overnight at  $120^\circ\text{C}$  until constant weight was recorded.

The weight loss percentage was calculated according to the equation: percentage of weight loss [%] =  $100 \cdot (m_0 - m_f) / m_0$ , where  $m_0$  is the initial sample mass and  $m_f$  is the final sample mass after the sample drying. The weight results of the samples consider the whole of the mass including the substrate and the coating.

To study the dissolution process of the glass coatings, pH changes were recorded at different time periods using a universal pH meter (Hach, Spain).

## 3. Results and discussion

### 3.1 Powder characterisation

The size distribution used for spray was micron-sized with  $D_{10} = 52\mu\text{m}$ ,  $D_{50} = 70\mu\text{m}$  and  $D_{90} = 110\mu\text{m}$ . The XRD pattern of the powder particles was the characteristic with amorphous structure.

The particles had irregular morphology as expected due to the route of fabrication. In addition, the cross section of the powders reveal full-dense particles (Fig. 1).

### 3.2 Coatings characterisation

Microstructure of the fabricated coatings can be observed in the cross-section micrographs showed in Fig 2. Due to the low thermal conductivity of the glass the particles are not completely molten during the spraying process even with the high temperatures of the plasma gas. Most of the particles are incompletely flattened when impacting the substrate providing this roughness to the substrate, which would be increased if the particle size of the powder is superior.

The cross sectional structure of the coatings reveals a significant amount of rounded cavities, this porosity is produced by volatilization of chemical components from the feedstock powder as reported previously for this glass composition [27].

The different coatings studied present a similar thickness, around  $150\mu\text{m}$ . Also the value of the surface roughness is almost equal for the diverse coatings, about  $13\mu\text{m}$ .

Particularly, the heat treated sample presents crystal structure and a major cohesion between the particles. However, the porosity and the thickness of the coating have not varied significantly.

XRD results confirm that the as-sprayed coatings are amorphous due to the fast cooling of the melted particles. As expected the coatings performed with carbon dioxide cooling present also an amorphous pattern, attributed also to the fast cooling of the particles.

There are crystalline phases in the patterns corresponding to the coatings heated at  $725^\circ\text{C}$  and  $800^\circ\text{C}$  (Fig. 3(A)). Both patterns have peaks corresponding to sodium calcium silicate ( $\text{Na}_6\text{Ca}_3\text{Si}_6\text{O}_{18}$ , Ref. code: 01-079-1089) observed also by other authors working with 45S5

glass [30,31]. Particularly, the peaks corresponding to the sodium calcium silicate are more intense for the samples treated at 800°C rather than 725°C.

Furthermore, the spectrum of the coating treated at 800°C reveals a secondary phase, corresponding to a sodium calcium phosphate silicate, identified as silicorhenanite ( $\text{Na}_2\text{Ca}_4(\text{PO}_4)_2\text{SiO}_4$ , Ref. code: 00-032-1053). Its crystallization starts at 800°C as reported by other authors [31,36]. It can be concluded that higher temperature results in more crystallinity for the coatings.

The adhesion test results presented in Fig 4 indicate that cooling during the spraying process does not increase the bond strength of the coating. Then this strategy does not result in an improvement of the adhesion. Higher values of adhesion strength have been measured for coatings heat treated. Samples heat treated at 800°C get a lower adhesion than the treated at 725°C, achieving for the latter a value of  $17.2 \pm 2.2$  MPa. With the heat treatment the coating stresses are reduced and crystallization is caused. As the glass is heated above the glass transition temperature a viscous state is achieved that produces better interparticle cohesion and a stress relaxation, which results in a stronger adhesion.

### 3.3 In vitro bioactivity study

In vitro tests were performed for 45S5 coatings, 45S5 with CO<sub>2</sub> cooling and 45S5 heat treated at 725°C due to the better adhesion results.

The representative morphologies of the coatings before and after the exposure to HBSS during different periods are shown in Fig. 5. When bioactive glasses are in contact with simulated body fluids a HCA layer is developed, it starts with the formation of small spheres that grow and aggregate with the soaking time, generating a dense layer. After 1 day of exposure a few apatite particles can be observed over all the surfaces. After 6 days the surface of all the coatings is fully covered by the HCA layer, which indicates a good bioactivity for all the coatings.



The XRD patterns after exposure in HBSS for 14 days indicate that the surfaces of the coatings were covered by HCA. All the patterns have peaks corresponding to hydroxyapatite ( $\text{Ca}_5(\text{PO}_4)_3(\text{OH})$ , Ref. code: 00-001-1008) (Fig. 3(B)). And the coatings without heat treatment present also peaks of calcium phosphate ( $\text{Ca}_2\text{O}_7\text{P}_2$ , Ref. code: 00-003-0605).

The bioactivity of a glass coating can be affected by many factors such as crystallinity, composition, porosity or specific surface area. Coatings obtained with cooling present less porosity, this fact could diminish the reactivity of the coating and diminish the degree of bioactivity. However, the difference is not enough to affect the formation of the apatite layer and the results reveal that  $\text{CO}_2$  cooling during spraying does not alter the bioactivity of the coatings.

Likewise the heat treatment does not affect the ability to form an apatite layer. It is expected that crystallinity can compromise the degree of bioactivity of the material, but partial crystallization not necessarily reduce it depending on the formed phases [37]. Previous studies have reported that the  $\text{Na}_6\text{Ca}_3\text{Si}_6\text{O}_{18}$  phase, detected in our coatings, is not affecting the HCA formation [38]. In our research, we have noticed that heat treated coatings allow the formation of the HCA layer, however a slight decrease in its formation rate can be seen. Particularly at 6 days (Fig. 5 (c,g,k)) less amount of apatite particles are present in heat treated coating.

The weight loss rate of coated samples after soaking in Tris-HCl solution is shown in Fig.6. The coatings obtained during cooling with carbon dioxide have similar degradation than the 45S5 coatings. It can be noticed that coatings heat treated at  $725^\circ\text{C}$  have significantly less degradation than the other ones, it can be attributed to the crystallinity.

In Fig.7 the results of the pH during soaking in Tris-HCl are shown. It help us to understand the ion exchange process between the coated samples and the Tris-HCl solution, the pH solution starts from 7.4 and increases to more than 7.8 for all the samples analysed. The increase of pH is higher the first hours, which indicates a fast ion exchange produced in the

solution. However, there is less variation from 72h to 120h possibly indicating a stabilization value at this period.

The 45S5 and 45S5 Cooling samples present a similar variation of pH with time, consequently the ion release is almost equal for both coatings. The heat treated coatings start with a higher pH value than the other ones. However, for the rest of the periods the pH value is lower for these coatings than for the amorphous ones. Another time, this behaviour can be attributed to the acquired crystallinity of the heat treated samples, that present less ion release from the coatings, corroborating the weight loss rate results.

#### 4. Conclusions

The effect of cooling with CO<sub>2</sub> during spraying maintain the amorphous structure of the coating. Otherwise the post heat treatment generates sodium calcium silicate crystalline phase to the samples heated at 725°C and 800°C and sodium calcium phosphate silicate phase when heating at 800°C.

The cooling process during spraying did not enhance the adhesion strength with the substrate, although with a post heat treatment high adhesion strengths were achieved due to the stress relaxation and the major cohesion achieved between particles. Higher values of adhesion strength were measured for coatings heat treated at 725°C reaching a value of  $17.2 \pm 2.2$  MPa.

The heat treatment provided a higher adhesion strength between the coating and the substrate, and preserved the bioactivity of the coatings in terms of HCA formation, but the kinetic of the HCA formation was slightly decreased. The development of a HCA layer in simulated body fluid solution is a positive indicator of the tendency of the coatings to support the mineralization process, however in terms of biological properties to prove the efficacy of the obtained coatings more studies should be developed, as cell tests.

Additionally, the degradation rate was lower for that coatings, due to the new arrangement of the glass structure. The results of the pH study in Tris-HCl solution corroborate that the ion release is higher for the amorphous coatings due to a more disrupted network.

## **Acknowledgements**

This work was supported by Generalitat de Catalunya (SGR-1777) and Spanish Government (MAT2016-76928-C2-1-R).

## References

- [1] P. Ducheyne, K.E. Healy, D.W. Grainger, D.W. Hutmacher, C.J. Kirkpatrick, Comprehensive biomaterials, 2011. <https://doi.org/10.1016/C2009-1-28384-5>.
- [2] M.G. Kaufman, J.D. Meaike, S.A. Izaddoost, Orthopedic Prosthetic Infections: Diagnosis and Orthopedic Salvage, Semin. Plast. Surg. 30 (2016) 66–72. <https://doi.org/10.1055/s-0036-1580730>.
- [3] L.L. Hench, The story of Bioglass®, in: J. Mater. Sci. Mater. Med., 2006. <https://doi.org/10.1007/s10856-006-0432-z>.
- [4] J.R. Jones, Review of bioactive glass: From Hench to hybrids, Acta Biomater. 9 (2013) 4457–4486. <https://doi.org/10.1016/j.actbio.2012.08.023>.
- [5] M. Montazerian, E. Dutra Zanotto, History and trends of bioactive glass-ceramics, J. Biomed. Mater. Res. - Part A. 104 (2016) 1231–1249. <https://doi.org/10.1002/jbm.a.35639>.
- [6] G. Kaur, V. Kumar, F. Baino, J.C. Mauro, G. Fickel, I. Evans, O. Bretcanu, Mechanical properties of bioactive glasses, ceramics, glass-ceramics and composites: State-of-the-art review and future challenges, Mater. Sci. Eng. C. 104 (2019) 109895. <https://doi.org/10.1016/j.msec.2019.109895>.
- [7] A. Hoppe, N.S. Güldal, A.R. Boccacini, A review of the biological response to ionic dissolution products from bioactive glasses and glass-ceramics, Biomaterials. 32 (2011) 2757–2774. <https://doi.org/10.1016/j.biomaterials.2011.01.004>.
- [8] I.D. Xynos, A.J. Edgar, L.D.M. K. Buttery, L.L. Hench, J.M. Polak, Gene-expression profiling of human osteoblasts following treatment with the ionic products of Bioglass® 45S5 dissolution, 2001. [https://doi.org/10.1002/1097-4636\(200105\)55:2<151::AID-JBM1001>3.0.CO;2-D](https://doi.org/10.1002/1097-4636(200105)55:2<151::AID-JBM1001>3.0.CO;2-D).
- [9] D.S. Brauer, Bioactive glasses - Structure and properties, Angew. Chemie - Int. Ed. 54 (2015) 4160–4181. <https://doi.org/10.1002/anie.201405310>.
- [10] S. Fagerlund, L. Hupa, M. Hupa, Dissolution patterns of biocompatible glasses in 2-Amino-2-hydroxy methyl- propane-1,3-diol (Tris) buffer, Acta Biomater. 9 (2013) 5400–5410. <https://doi.org/10.1016/j.actbio.2012.08.051>.
- [11] S. Lopez-Esteban, E. Saiz, S. Fujino, T. Oku, K. Suganuma, A.P. Tomsia, Bioactive glass coatings for orthopedic metallic implants, J. Eur. Ceram. Soc. 23 (2003) 2921–2930. [https://doi.org/10.1016/S0955-2219\(03\)00303-0](https://doi.org/10.1016/S0955-2219(03)00303-0).
- [12] L.L. Hench, Chronology of Bioactive Glass Development and Clinical Applications, New J. Glas. Ceram. 03 (2013) 67–73. <https://doi.org/10.4236/njgc.2013.32011>.
- [13] M. Peltola, K. Aitasalo, J. Suonpää, M. Varpula, A. Yli-Urpo, Bioactive glass S53P4 in frontal sinus obliteration: A long-term clinical experience, Head Neck. 28 (2006) 834–841. <https://doi.org/10.1002/hed.20436>.
- [14] B. Ilharreborde, E. Morel, F. Fitoussi, A. Presedo, P. Souchet, G.F. Penneçot, K. Mazda, Bioactive glass as a bone substitute for spinal fusion in adolescent idiopathic scoliosis: A comparative study with iliac crest autograft, J. Pediatr. Orthop. 28 (2008)

347–351. <https://doi.org/10.1097/BPO.0b013e318168d1d4>.

- [15] F. Carinci, A. Palmieri, M. Martinelli, V. Perrotti, A. Piattelli, G. Brunelli, M. Arlotti, F. Pezzetti, Genetic portrait of osteoblast-like cells cultured on PerioGlas, *J. Oral Implantol.* 33 (2007) 327–333. [https://doi.org/10.1563/1548-1336\(2007\)33\[327:GPOOCC\]2.0.CO;2](https://doi.org/10.1563/1548-1336(2007)33[327:GPOOCC]2.0.CO;2).
- [16] J.R. Jones, D.S. Brauer, L. Hupa, D.C. Greenspan, Bioglass and Bioactive Glasses and Their Impact on Healthcare, *Int. J. Appl. Glas. Sci.* 7 (2016) 423–434. <https://doi.org/10.1111/ijag.12252>.
- [17] B.J. Tai, Z. Bian, H. Jiang, D.C. Greenspan, J. Zhong, A.E. Clark, M.Q. Du, Anti-gingivitis effect of a dentifrice containing bioactive glass (NovaMin®) particulate, *J. Clin. Periodontol.* 33 (2006) 86–91. <https://doi.org/10.1111/j.1600-051X.2005.00876.x>.
- [18] L. Sun, C.C. Berndt, K.A. Gross, A. Kucuk, Material fundamentals and clinical performance of plasma-sprayed hydroxyapatite coatings: a review., *J. Biomed. Mater. Res.* 58 (2001) 570–592. <https://doi.org/10.1002/jbm.b.10056>.
- [19] H. Melero, J. Fernández, S. Dosta, J. Guilemany, Caracterización de nuevos recubrimientos biocompatibles de hidroxiapatita-TiO<sub>2</sub> obtenidos mediante proyección térmica de alta velocidad, *Bol. La Soc. Esp. Ceram. y Vidr.* 50 (2011) 59–64. <https://doi.org/10.3989/cyv.082011>.
- [20] E. Kergourlay, D. Grossin, N. Cinca, C. Jesse, S. Dosta, G. Bertrand, I. Garcia, J.M. Guilemany, C. Rey, First Cold Spraying of Carbonated Biomimetic Nanocrystalline Apatite on Ti6Al4V: Physical-Chemical, Microstructural, and Preliminary Mechanical Characterizations, *Adv. Eng. Mater.* 18 (2016) 496–500. <https://doi.org/10.1002/adem.201500409>.
- [21] V. Cannillo, F. Pierli, S. Sanjath, C. Siligardi, Thermal and physical characterisation of apatite/wollastonite bioactive glass-ceramics, *J. Eur. Ceram. Soc.* 29 (2009) 611–619. <https://doi.org/10.1016/j.jeurceramsoc.2008.06.034>.
- [22] V.L. Calvo, M.V. Cabedo, E. Bannier, E.C. Recacha, A.R. Boccaccini, L.C. Arias, E.S. Vilches, 45S5 bioactive glass coatings by atmospheric plasma spraying obtained from feedstocks prepared by different routes, *J. Mater. Sci.* 49 (2014) 7933–7942. <https://doi.org/10.1007/s10853-014-8519-2>.
- [23] S. Bano, I. Ahmed, D.M. Grant, A. Nommeots-Nomm, T. Hussain, Effect of processing on microstructure, mechanical properties and dissolution behaviour in SBF of Bioglass (45S5) coatings deposited by Suspension High Velocity Oxy Fuel (SHVOF) thermal spray, *Surf. Coatings Technol.* 372 (2019) 229–238. <https://doi.org/10.1016/j.surfcoat.2019.05.038>.
- [24] A. Cattini, D. Bellucci, A. Sola, L. Pawłowski, V. Cannillo, Functional bioactive glass topcoats on hydroxyapatite coatings: Analysis of microstructure and in-vitro bioactivity, *Surf. Coatings Technol.* 240 (2014) 110–117. <https://doi.org/10.1016/j.surfcoat.2013.12.023>.
- [25] E. Cañas, M.J. Orts, A.R. Boccaccini, E. Sánchez, Solution Precursor Plasma Spraying (SPPS): A novel and simple process to obtain bioactive glass coatings, *Mater. Lett.* 223 (2018) 198–202. <https://doi.org/10.1016/j.matlet.2018.04.031>.

- [26] G. Bolelli, D. Bellucci, V. Cannillo, R. Gadow, A. Killinger, L. Lusvardi, P. Müller, A. Sola, Comparison between Suspension Plasma Sprayed and High Velocity Suspension Flame Sprayed bioactive coatings, *Surf. Coatings Technol.* 280 (2015) 232–249. <https://doi.org/10.1016/j.surfcoat.2015.08.039>.
- [27] O. Rojas, M. Prudent, M.E. López, F. Vargas, H. Ageorges, Influence of Atmospheric Plasma Spraying Parameters on Porosity Formation in Coatings Manufactured from 45S5 Bioglass® powder, *J. Therm. Spray Technol.* 29 (2020) 185–198. <https://doi.org/10.1007/s11666-019-00952-3>.
- [28] E. Verné, M. Miola, C. Vitale Brovarone, M. Cannas, S. Gatti, G. Fucile, G. Maina, A. Massé, S. Di Nunzio, Surface silver-doping of biocompatible glass to induce antibacterial properties. Part I: Massive glass, *J. Mater. Sci. Mater. Med.* 20 (2009) 733–740. <https://doi.org/10.1007/s10856-008-3617-9>.
- [29] S.D. Newman, N. Lotfibakhshaiesh, M. O'Donnell, X.M. Walboomers, N. Horwood, J.A. Jansen, A.A. Amis, J.P. Cobb, M.M. Stevens, Enhanced Osseous Implant Fixation with Strontium-Substituted Bioactive Glass Coating, *Tissue Eng. Part A.* 20 (2014) 1850–1857. <https://doi.org/10.1089/ten.tea.2013.0304>.
- [30] V. Cannillo, A. Sola, Different approaches to produce coatings with bioactive glasses: Enamelling vs plasma spraying, *J. Eur. Ceram. Soc.* 30 (2010) 2031–2039.
- [31] D. Bellucci, V. Cannillo, A. Sola, An overview of the effects of thermal processing on bioactive glasses, *Sci. Sinter.* 42 (2010) 327–329. <https://doi.org/10.2298/SOS1007327B>.
- [32] A. Ducato, L. Fratini, M. La Cascia, G. Mazzola, An automated visual inspection system for the classification of the phases of Ti-6Al-4V titanium alloy, in: *Lect. Notes Comput. Sci. (Including Subser. Lect. Notes Artif. Intell. Lect. Notes Bioinformatics)*, 2013: pp. 362–369. [https://doi.org/10.1007/978-3-642-40246-3\\_45](https://doi.org/10.1007/978-3-642-40246-3_45).
- [33] Q. Zhao, D. He, L. Zhao, X. Li, In-vitro study of microplasma sprayed hydroxyapatite coatings in Hanks balanced salt solution, *Mater. Manuf. Process.* 26 (2011) 175–180. <https://doi.org/10.1080/10426914.2010.498071>.
- [34] J.A. Rincón-López, J.A. Hermann-Muñoz, N. Cinca-Luis, B. Garrido-Domínguez, I. García-Cano, J.M. Guilemany-Casadamon, J.M. Alvarado-Orozco, J. Muñoz-Saldaña, Preferred Growth Orientation of Apatite Crystals on Biological Hydroxyapatite Enriched with Bioactive Glass: A Biomimetic Behavior, *Cryst. Growth Des.* 19 (2019) 5005–5018. <https://doi.org/10.1021/acs.cgd.9b00268>.
- [35] S.A. Omar, J. Ballarre, Y. Castro, E. Martínez Campos, W. Schreiner, A. Durán, S.M. Cere, 58S and 68S sol-gel glass-like bioactive coatings for enhancing the implant performance of AZ91D magnesium alloy, *Surf. Coatings Technol.* 400 (2020). <https://doi.org/10.1016/j.surfcoat.2020.126224>.
- [36] L. Lefebvre, J. Chevalier, L. Gremillard, R. Zenati, G. Thollet, D. Bernache-Assolant, A. Govin, Structural transformations of bioactive glass 45S5 with thermal treatments, *Acta Mater.* 55 (2007) 3305–3313. <https://doi.org/10.1016/j.actamat.2007.01.029>.
- [37] J. Chevalier, L. Gremillard, Ceramics for medical applications: A picture for the next 20 years, *J. Eur. Ceram. Soc.* 29 (2009) 1245–1255. <https://doi.org/10.1016/j.jeurceramsoc.2008.08.025>.

- [38] S. Grasso, R.K. Chinnam, H. Porwal, A.R. Boccaccini, M.J. Reece, Low temperature spark plasma sintering of 45S5 Bioglass®, J. Non. Cryst. Solids. 362 (2013) 25–29. <https://doi.org/10.1016/j.jnoncrysol.2012.11.009>.

Table 1. Plasma spraying parameters

<b>Spraying parameters</b>	<b>Bioactive glass coatings</b>
Argon plasma gas flow rate (slpm)*	35
Hydrogen plasma gas flow rate (slpm)*	12
Spray distance (mm)	125
Argon powder carrier gas (slpm)*	4
Injection angle (°)	90
Current (A)	600
Voltage (V)	65
Spray cycles	5
*Standard litre per minute	



**List of figure captions**

**Figure 1.** SEM micrographs of the free surface (A) and cross section (B) of the 45S5 powder.

**Figure 2.** Cross section of the coatings: 45S5 as-sprayed (A), 45S5 with cooling (B) and with heat treatment to 725°C.

**Figure 3.** X-ray spectra of A) powder and coatings as-sprayed, with heat treatment to 725°C and 800°C and B) after being soaked in HBSS for 14 days.

**Figure 4.** Tensile strength results of the different coatings.

**Figure 5.** Morphology of samples as-sprayed (A,E,I), after 1 (B,F,J), 6 (C,G,K) and 14 (D,H,L) days of exposure to HBSS solution.

**Figure 6.** Weight loss rate of coated samples after soaking in Tris-HCl.

**Figure 7.** pH values of coated samples during soaking in Tris-HCl for different periods.

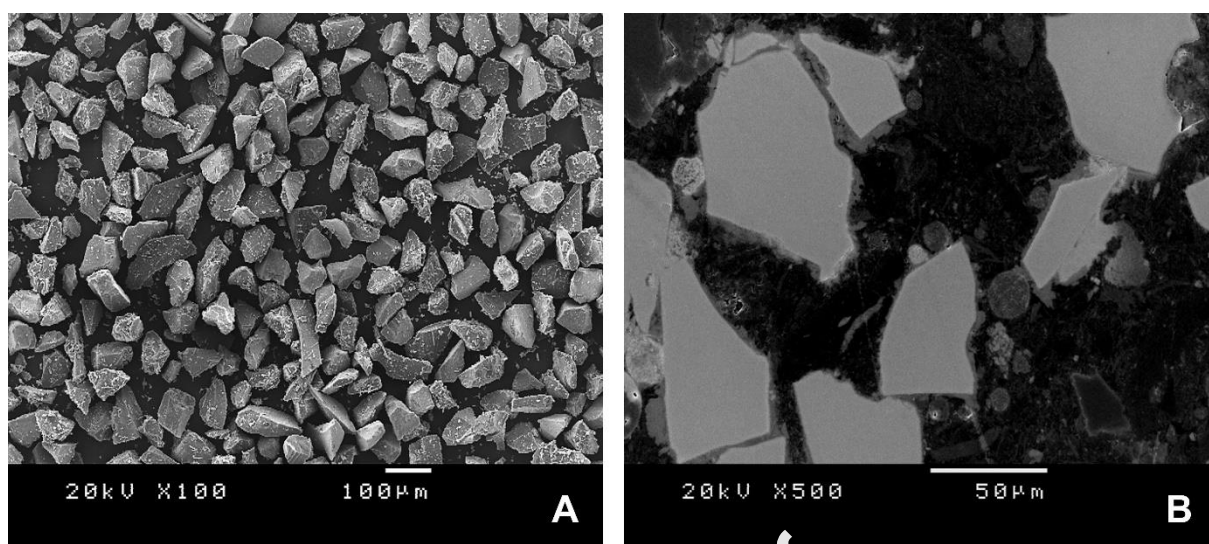
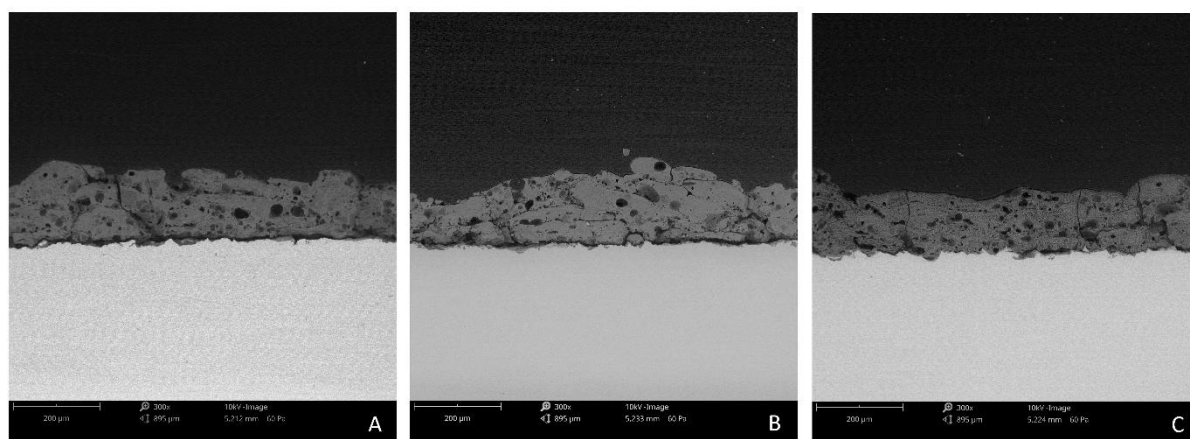


Figure 1

**Figure 2**

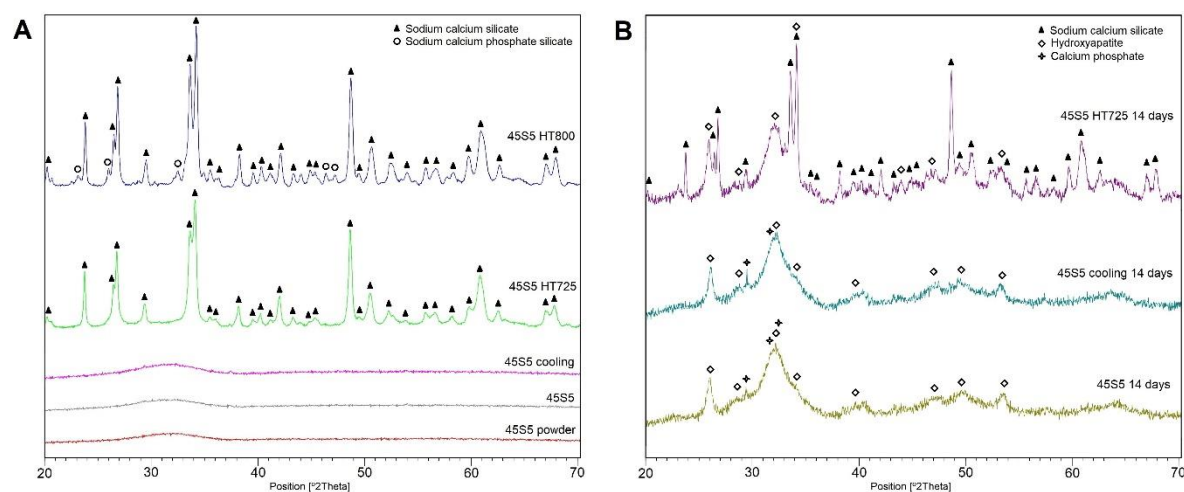
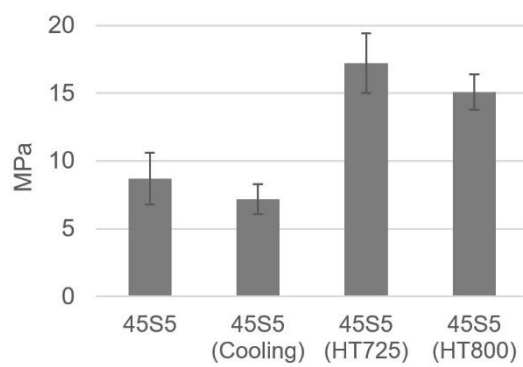
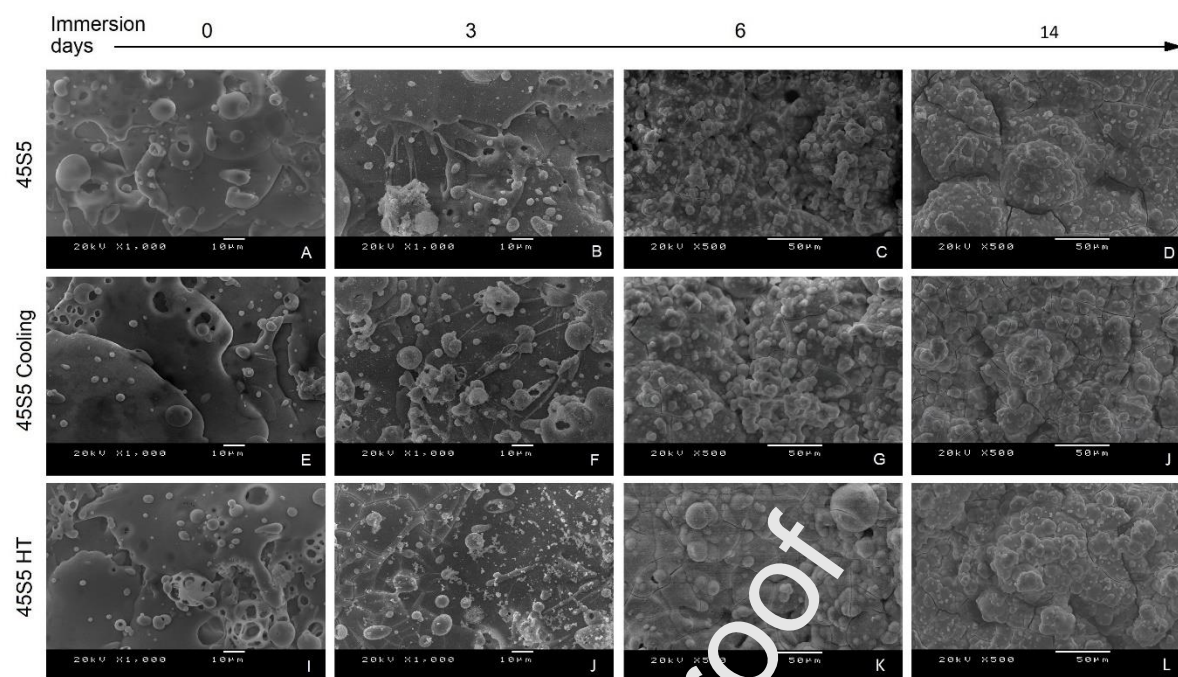
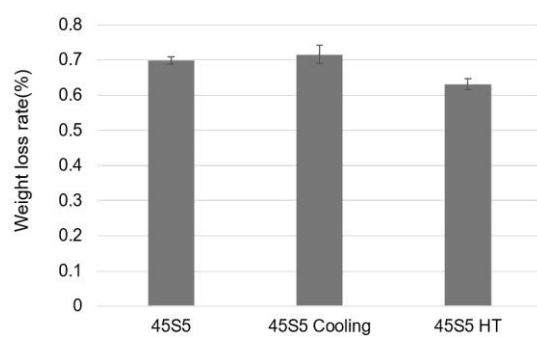
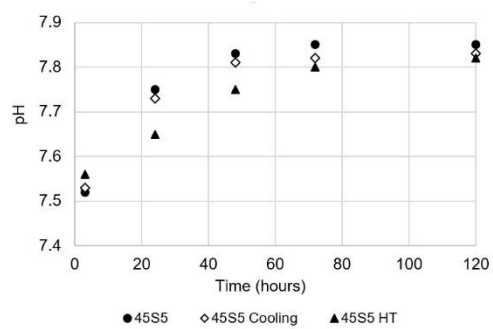


Figure 3

**Figure 4**



**Figure 6**

**Figure 7**



### **Credit Author Statement**

Conceptualization; I.G. Cano

Data curation; B. Garrido and S. Dosta

Formal analysis; B. Garrido

Funding acquisition; I.G. Cano and S. Dosta

Investigation; B. Garrido and S. Dosta

Methodology; B. Garrido, I.G. Cano and S. Dosta

Project administration; I.G. Cano

Resources; I.G. Cano and S. Dosta

Supervision; I.G. Cano and S. Dosta

Validation; B. Garrido, I.G. Cano and S. Dosta

Visualization; B. Garrido and S. Dosta

Roles/Writing - original draft; B. Garrido

Writing - review & editin; I.G. Cano and S. Dosta

**Declaration of interests:**

☒ The authors declare that they have no known competing financial interests or personal relationships that could have appeared to influence the work reported in this paper.

☐ The authors declare the following financial interests/personal relationships which may be considered as potential competing interests:

### Highlights

- Degradation rate of the 45S5 coatings is faster for the amorphous ones.
- The adherence of the bioactive glass coatings was enhanced after heat treatments.
- The coatings were fully covered by hydroxycarbonate apatite after 6 days of Hank's solution immersion.

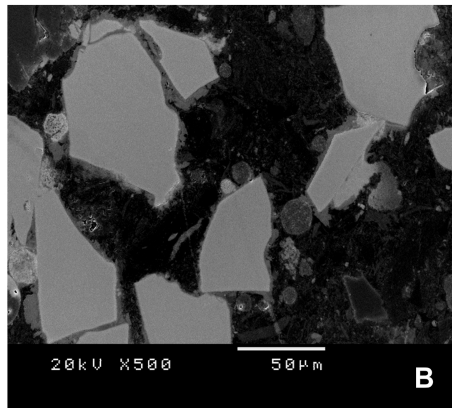
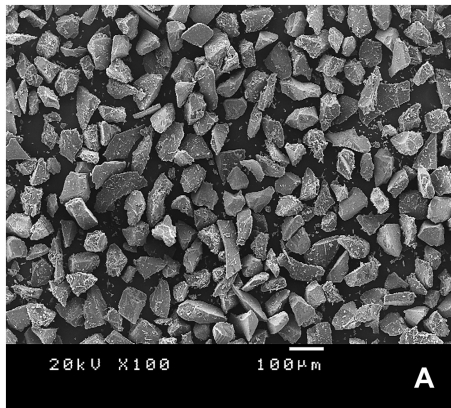


Figure 1

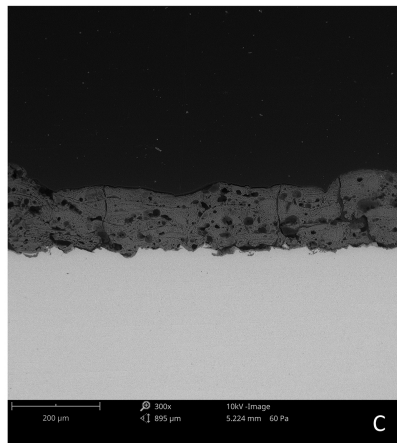
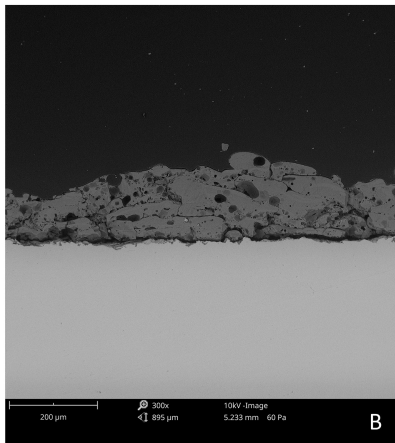
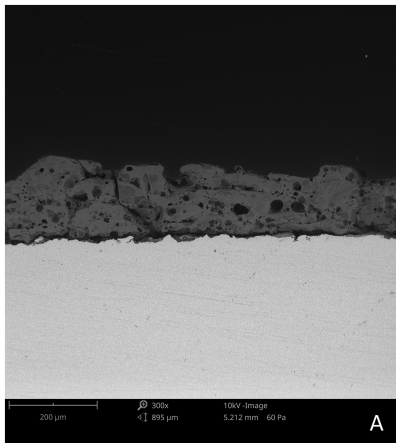


Figure 2

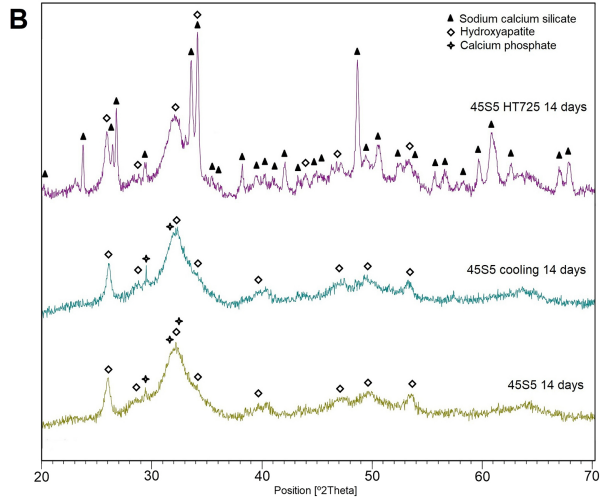
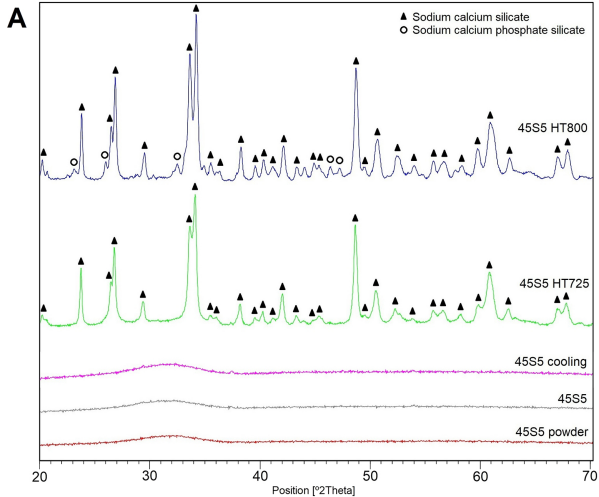


Figure 3

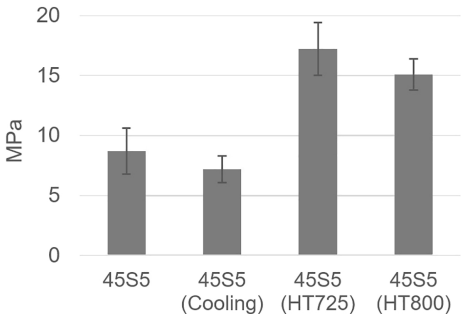


Figure 4

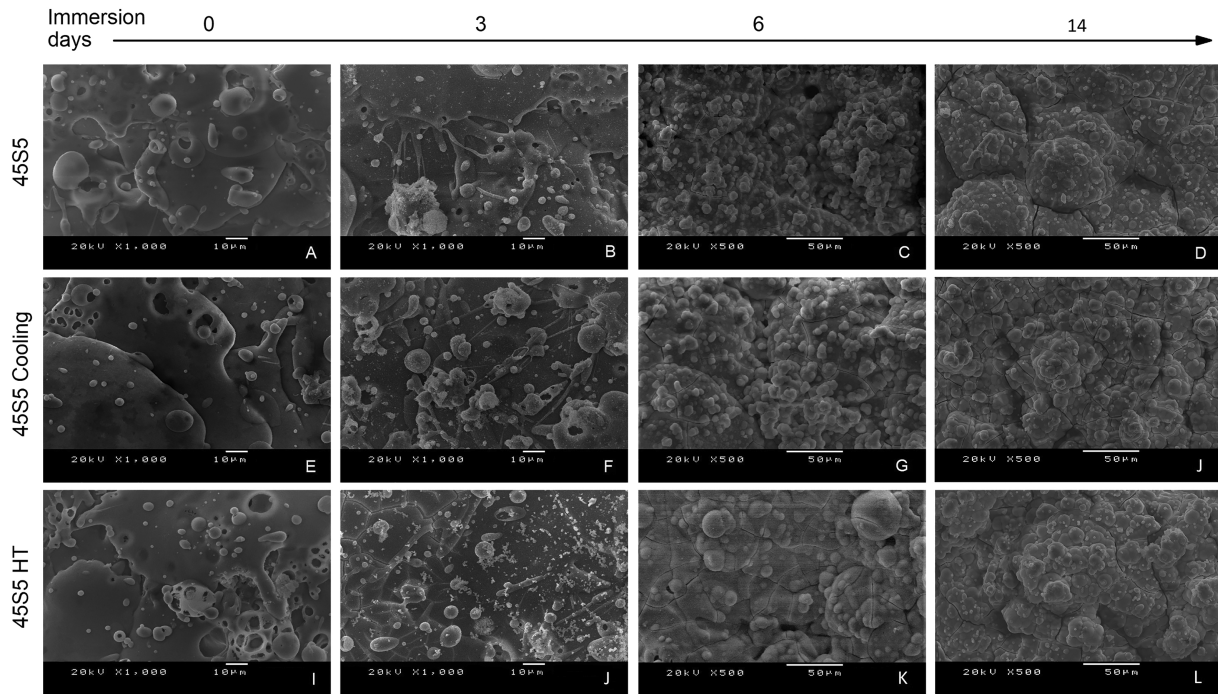


Figure 5



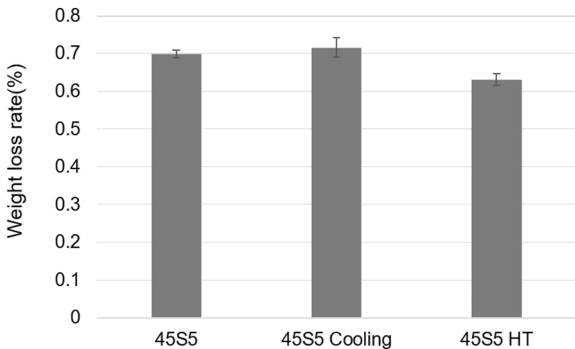


Figure 6

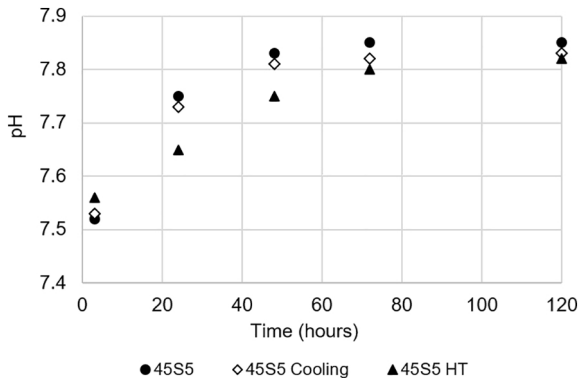


Figure 7